Theor Chem Acc (2009) 124:123–137
DOI 10.1007/s00214-009-0591-3

REGULAR ARTICLE

Radical reaction HCNO + ^{3}NH: a mechanistic study

Yan Li · Hui-ling Liu · Yan-bo Sun · Zhuo Li · Xu-ri Huang · Chia-chung Sun

Received: 2 April 2009 / Accepted: 14 May 2009 / Published online: 31 May 2009

Abstract The complex triplet potential energy surface for the reaction of HCNO with NH is investigated at the G3B3 level using the B3LYP/6-311++G(d,p), and QCISD/6-311++G(d,p) geometries. Various possible isomerization and dissociation pathways are probed. The initial association between HCNO and NH is found to be carbon to nitrogen attack leading to HNCHNO **2a**, which can convert to **2b**, **2c**, and **2d**. Subsequently, 1,4-H-shift of **2a** to form NCHNOH **3a** followed by dissociation to **P$_2$**(^{1}HCN + ^{3}HON) is the most feasible pathway. Much less competitively, **2d** undergoes successive 1,3-H-shift and C-N cleavage to form HNCNOH **8b**, and then to product **P$_3$**(^{1}HNC + ^{3}HON), the second feasible pathway. **8b** can alternatively isomerize to **8c** followed by N–O bond rupture to generate **P$_6$**(^{2}OH + ^{2}HNCN), the lesser followed feasible pathway. In addition, **2b** takes continuously 1,3- and 1,2-H-shift to form NC(H)NHO **6a**, then to ONHCNH **7a** which can convert to **7b**. Eventually, **7b** may take C-N bond fission to produce **P$_5$**(^{1}HNC + ^{3}HNO), the least feasible pathway. The present paper may be helpful for future experimental identification of the product distributions for the title reaction, and may be helpful to deeply understand the mechanism of the title reaction.

Keywords Theoretical calculations · Reaction mechanism · Potential energy surface (PES) · Fulminic acid (HCNO) imidogen radical (^{3}NH)

Y. Li · H. Liu · Y. Sun · Z. Li · X. Huang (✉) · C. Sun
State Key Laboratory of Theoretical and Computational Chemistry, Institute of Theoretical Chemistry, Jilin University, 130023 Changchun, People's Republic of China
e-mail: snow2007liyan@163.com

1 Introduction

Fulminic acid (HCNO) plays an important role in the combustion chemistry due to its involvement in the NO-reburning process for the reduction of NO*x* pollutants [1]. It can be formed in combustion processes either by CH_2 reactions with NO [2–5] or by HCCO reactions with NO [6–11]. Thus, it is of great significance to learn the behavior of the HCNO radical for environmental protection. Up to now, it has been the subject of several spectroscopic investigations [12, 13]. Besides, a number of experimental and theoretical studies have been reported on the HCNO reactions with a variety of species such as O(^{3}P) [14–16], OH [17, 18], NCO [19–21], CN [22, 23], and H [24], etc.

On the other hand, the ground-state imidogen radical, ^{3}NH has attracted considerable attentions of spectroscopists, experimenters, and theoreticians because it has been predicted to be of great importance to understand the nitrogen chemistry in flames [25, 26] as well as the De-NOx and RAPRENO*x* combustion processes [27]. Up to now, a large number of experimental and theoretical studies have been reported on the spectra of ^{3}NH [28–31] and it reactions with H [32], CH [33], C_2 [34], HNCO [35], CH_4 [36], C_2H_4 [36, 37], CH_3 [38], H_2 [39], H_2O [39], and CO_2 [39]. Furthermore, we notice that ^{3}NH radical is isoelectronic with ^{3}O and the reaction between HCNO and ^{3}O has been studied extensively [14–16]. In contrast to the rich knowledge of the HCNO + ^{3}O reaction, the HCNO + ^{3}NH reaction has received little attention. To our best knowledge, neither experimental- nor theoretical studies have been reported on the reaction of HCNO + ^{3}NH up to now. Thus, in the present paper, we report the first study on the chemical reactivity of HCNO towards ^{3}NH by means of quantum chemical

calculations. Our main goal of the present paper is (1) to provide the elaborated isomerization and dissociation channels, and (2) to identify the product distribution and thereby to provide a base for future dynamical calculations.

2 Theoretical methods

All calculations are carried out using the GAUSSIAN98 and GAUSSIAN03 program packages [40, 41]. The optimized geometries and harmonic frequencies of the reactant, products, intermediates, and transition states are obtained at the B3LYP/6-311++G(d,p) level. Single-point calculations of all species are performed at the G3B3 [42, 43] level using the B3LYP/6-311++G(d,p)-optimized geometries and scaled B3LYP/6-311++G(d,p)-zero-point energies. Connections of the transition states between designated isomers are confirmed by intrinsic reaction coordinate (IRC) calculations at the B3LYP/6-311++G(d,p) level. For some critical structures, the QCISD/6-311++G(d,p) is used to optimize geometries followed by G3B3 single-point energy calculations.

3 Results and discussion

Figure 1 depicts the structures of reactant, and various products. Figures 2 and 3 depict the structures of isomers and transition states, respectively. The schematic potential energy surface (PES) of the HCNO + ^{3}NH reaction at the G3B3//B3LYP/6-311++G(d,p) level is presented in Figs. 4a, b and Table 1 lists the energetic data of the reactant, products, and isomers whereas those of the transitions states are shown in Table 2. For easier discussion, the total energy of the reactant HCNO + ^{3}NH is set as zero for reference. The symbol **TSm/n** is used to denote the transition state connecting isomers **m** and **n**. Unless otherwise specified, the G3B3//B3LYP/6-311++G(d,p) energies are used throughout. Moreover, for assessment of the G3B3//B3LYP/6-311++G(d,p) results, the optimized QCISD/6-311++G(d,p) geometries of the critical structures are shown in Fig. 5, and the corresponding G3B3//QCISD/6-311++G(d,p) energies are listed in Table 3.

3.1 Entrance channels

The attack of the ^{3}NH radical on HCNO may have three possible patterns, that is, (i) quasi-direct H-abstraction

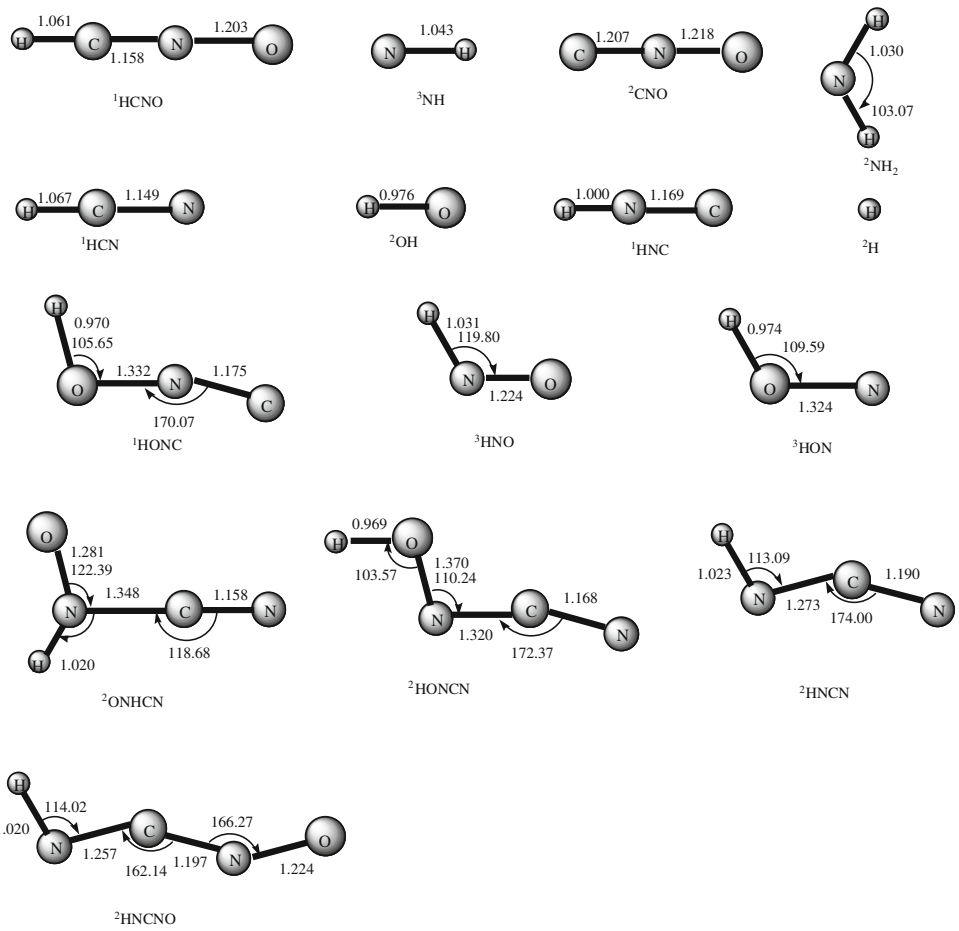

Fig. 1 The optimized structures of the reactant and products at the B3LYP/6-311++G(d,p) level. Distances are given in angstroms and angles in degrees

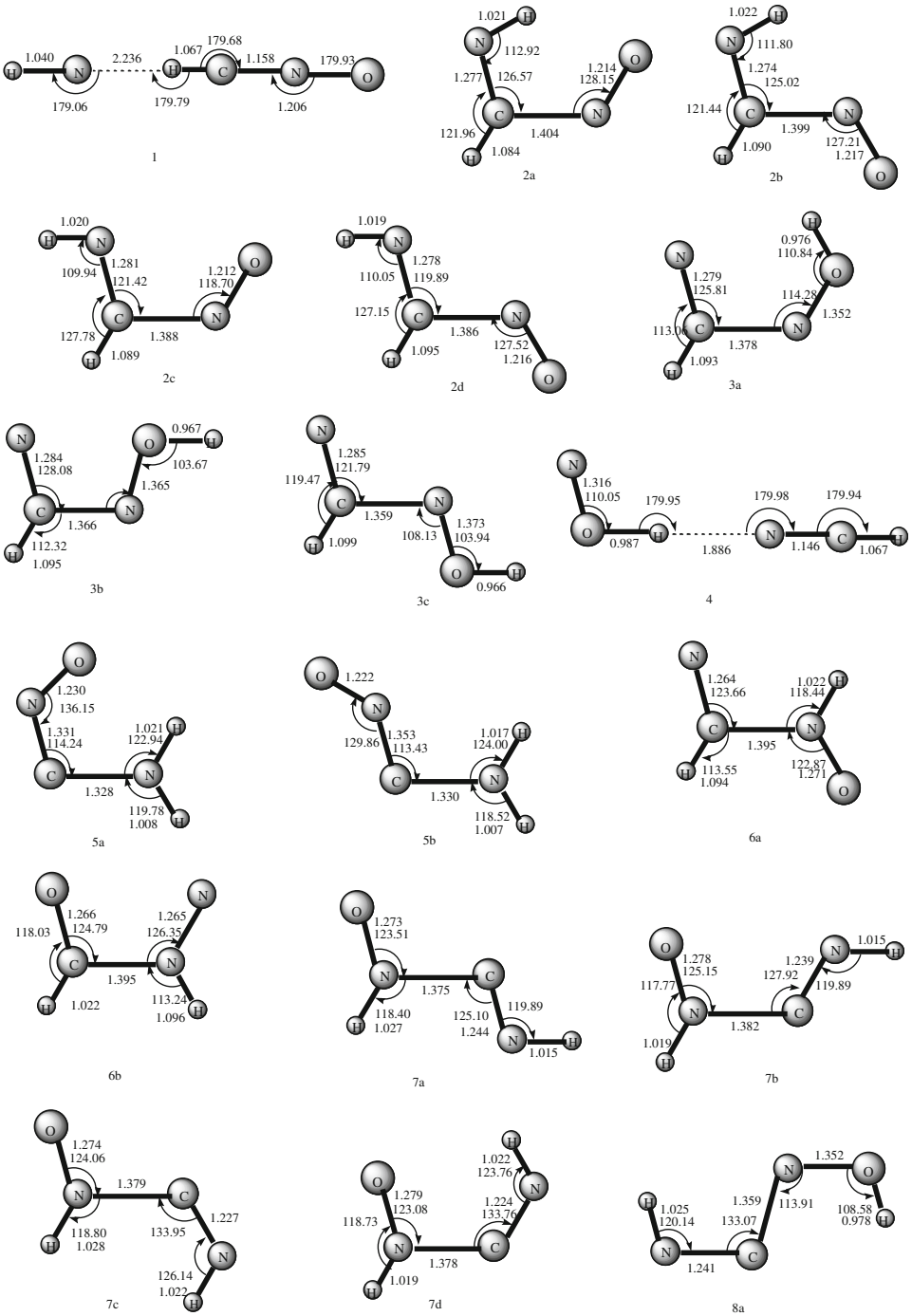

Fig. 2 The optimized structures of the intermediates at the B3LYP/6-311++G(d,p) level. Distances are given in angstroms and angles in degrees

leading to product $\mathbf{P_1}(^2NH_2 + {}^2CNO)$ (13.1) via **TS1/18** (20.6) and postreaction complex HNH···CNO **Com18** (11.9); (ii) C-addition to form HNCHNO **2a** (–58.5) via **TS1/2a** (2.9); (iii) N-addition to form HCN(O)NH **19a** (8.5), **19b** (10.7), **19c** (16.1), and **19d** (11.9) via **TS17/19a** (43.5), **TS17/19b** (34.0), **TS17/19c** (35.5), and **TS17/19d** (41.2), respectively. Note that the values in parentheses are relative energies in kcal/mol with reference to **R** (HCNO + ^{3}NH)(0.0). Interestingly, two weakly bound complexes HN···HCNO **Com1** (–2.9) and NH···ONCH **Com17** (–1.8) are first met prior to the above three channels. Channels (i) and (ii) start from **Com1**, while channel (iii) starts from **Com17**. Obviously, only the C-addition channel (ii) is of interest. It is both thermodynamically and kinetically much more competitive than the other channels. Note that the low-lying intermediate HNCHNO **2** has four isomeric forms **2a** (–58.5), **2b** (–58.0), **2c** (–56.9), and **2d** (–57.2); optimization of the transition states **TS1/2b**,

Fig. 2 continued

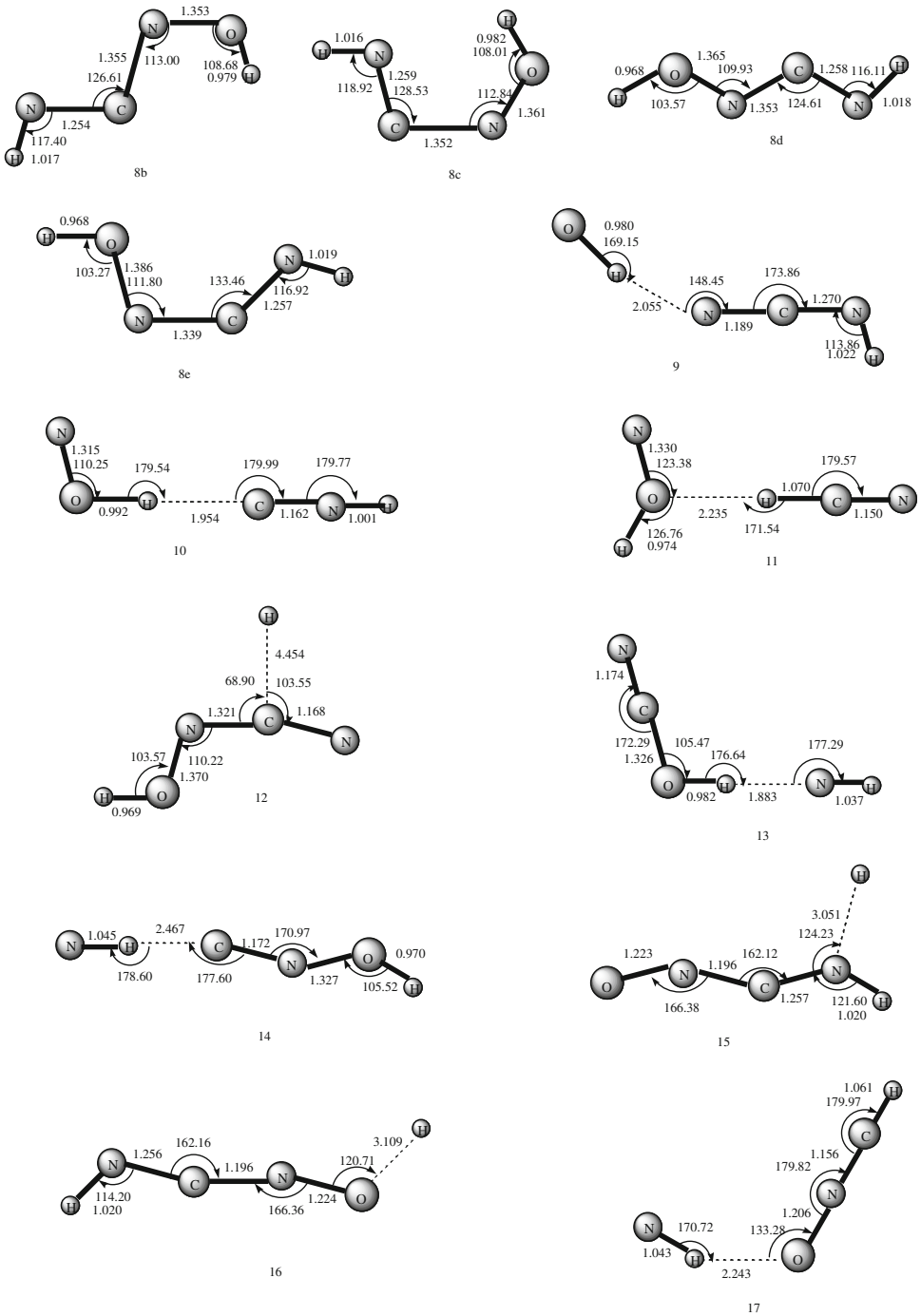

TS1/2c, and **TS1/2d** cannot succeed despite extensive attempts. For simplicity, the *cis-trans* isomerization between **2a**, **2b**, **2c**, and **2d** is not shown in the PES.

3.2 Reaction channels

Starting from the most favorable entrance isomer HNCHNO **2a**, nine products can be obtained via successive isomerization and dissociation pathways. The relative energies of these nine products at G3B3//B3LYP/6-311++G(d,p) level increase as follows: $\mathbf{P_2}$ (^{1}HCN + ^{3}HON) (–42.0) → $\mathbf{P_6}$ (^{2}OH + ^{2}HNCN) (–39.5) → $\mathbf{P_5}$ (^{1}HNC + ^{3}HNO) (–34.3) → $\mathbf{P_3}$ (^{1}HNC + ^{3}HON) (–27.3) → $\mathbf{P_8}$ (^{2}HONCN + ^{2}H) (–9.3) → $\mathbf{P_7}$ (^{2}ONHCN + ^{2}H) (–8.4) → $\mathbf{P_4}$ (^{2}HNCNO + ^{2}H) (3.9) → $\mathbf{P_1}$ (^{2}NH$_2$ + ^{2}CNO) (13.1) → $\mathbf{P_9}$ (^{1}HONC + ^{3}NH) (15.4). Obviously, products $\mathbf{P_1}$, $\mathbf{P_4}$ and $\mathbf{P_9}$ with positive relative energies are surely thermodynamically not accessible. On the other hand, products $\mathbf{P_7}$ and $\mathbf{P_8}$ lie much higher

Fig. 2 continued

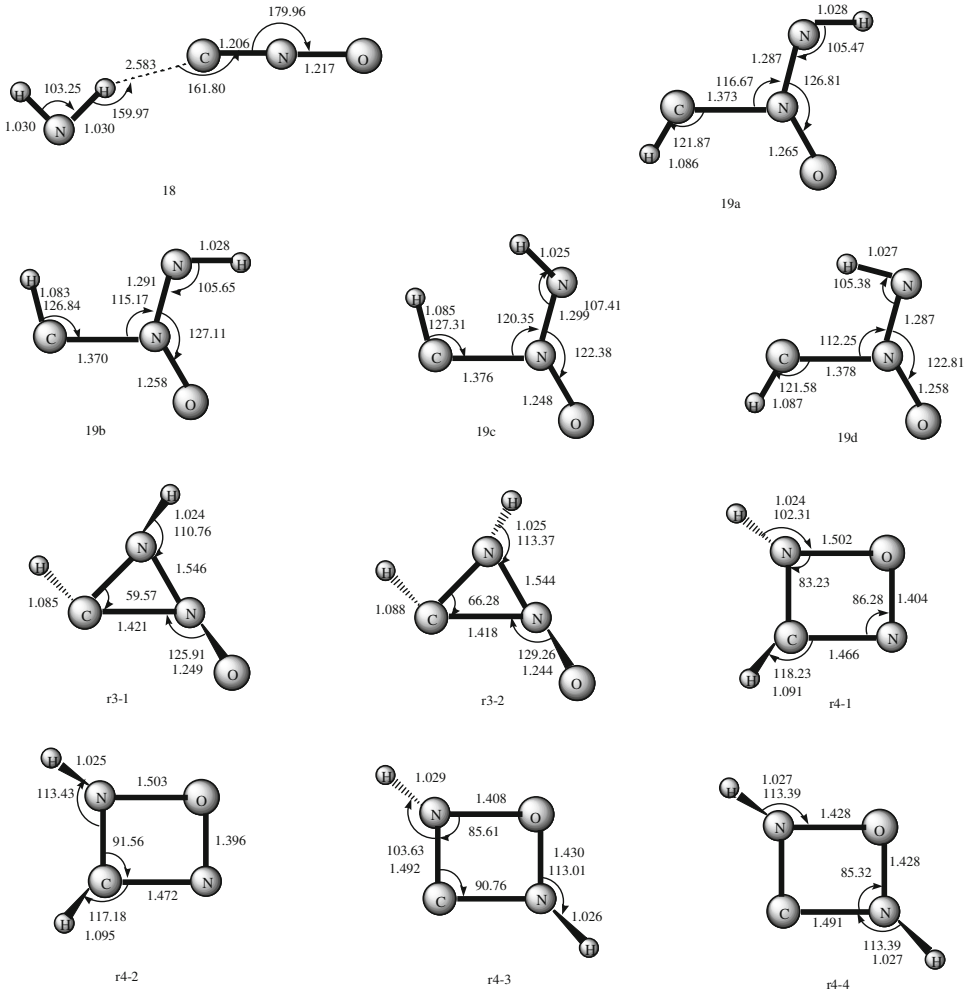

than $\mathbf{P_2}$, $\mathbf{P_3}$, $\mathbf{P_5}$, and $\mathbf{P_6}$, which thermodynamically prevents their experimental observation with detected yields respect to $\mathbf{P_2}$, $\mathbf{P_3}$, $\mathbf{P_5}$, and $\mathbf{P_6}$. In the following parts, we will first discuss the favorable reaction channels which associated with the formation of $\mathbf{P_2}$, $\mathbf{P_3}$, $\mathbf{P_5}$, and $\mathbf{P_6}$.

3.2.1 *Formation pathways of* $\boldsymbol{P_2}$*(*^{1}*HCN* + ^{3}*HON)*

$\mathbf{P_2}$(^{1}HCN + ^{3}HON) is the lowest-lying product. From Fig. 4a, we find that two pathways are energetically possible as follows:

Path $\mathbf{P_2(1)}$**R** → **1** → **2a** → **3a** → $\mathbf{P_2}$

Path $\mathbf{P_2(2)}$**R** → **1** → **2a** → **4** → $\mathbf{P_2}$

HNCHNO **2a** can undergo either 1,4-H-shift to form NCHNOH **3a** followed by C-N bond rupture to give $\mathbf{P_2}$ as in **Path** $\mathbf{P_2(1)}$, or a concerted 1,4-H-shift along with C-N bond rupture to generate the weakly bound complex NOH···NCH **4** before the final product $\mathbf{P_2}$ as in **Path** $\mathbf{P_2(2)}$.

In **Path** $\mathbf{P_2(1)}$, two barriers need to be climbed; from **2a** to $\mathbf{P_2}$, i.e., 39.2 and 11.4 kcal/mol for **2a** → **3a** and **3a** → $\mathbf{P_2}$ conversions, respectively. Yet, in **Path** $\mathbf{P_2(2)}$, one high barrier 61.5 kcal/mol for **2a** → **4** conversion is needed. Moreover, **TS2a/4 in Path** $\mathbf{P_2(2)}$ is 3.0 kcal/mol higher in energy than reactant **R**(HCNO + ^{3}NH). Thus, we expect that **Path** $\mathbf{P_2(1)}$ should be more competitive than **Path** $\mathbf{P_2(2)}$.

3.2.2 *Formation pathways of* $\boldsymbol{P_3}$*(*^{1}*HNC* + ^{3}*HON)*

There are four feasible pathways to form $\mathbf{P_3}$ which can be written as follows:

Path $\mathbf{P_3(1)}$**R** → **2a** → **2b** → **8a** → **10** → $\mathbf{P_3}$

Path $\mathbf{P_3(2)}$**R** → **2a** → **2c** → **2d** → **8b** → $\mathbf{P_3}$

Path $\mathbf{P_3(3)}$**R** → **2a** → **2c** → **2d** → **8b** → **8d** → $\mathbf{P_3}$

Path $\mathbf{P_3(4)}$**R** → **2a** → **2c** → **2d** → **8b** → **8c** → **8e** → **8d** → $\mathbf{P_3}$

The formation pathway of HNCHNO **2** (**2a**, **2b**, **2c**, and **2d**) has been discussed previously. **2b** requires a 1,3-H-shift to form HNCNOH **8a**; then **8a** undergoes C-N bond fission leading to the weakly bound

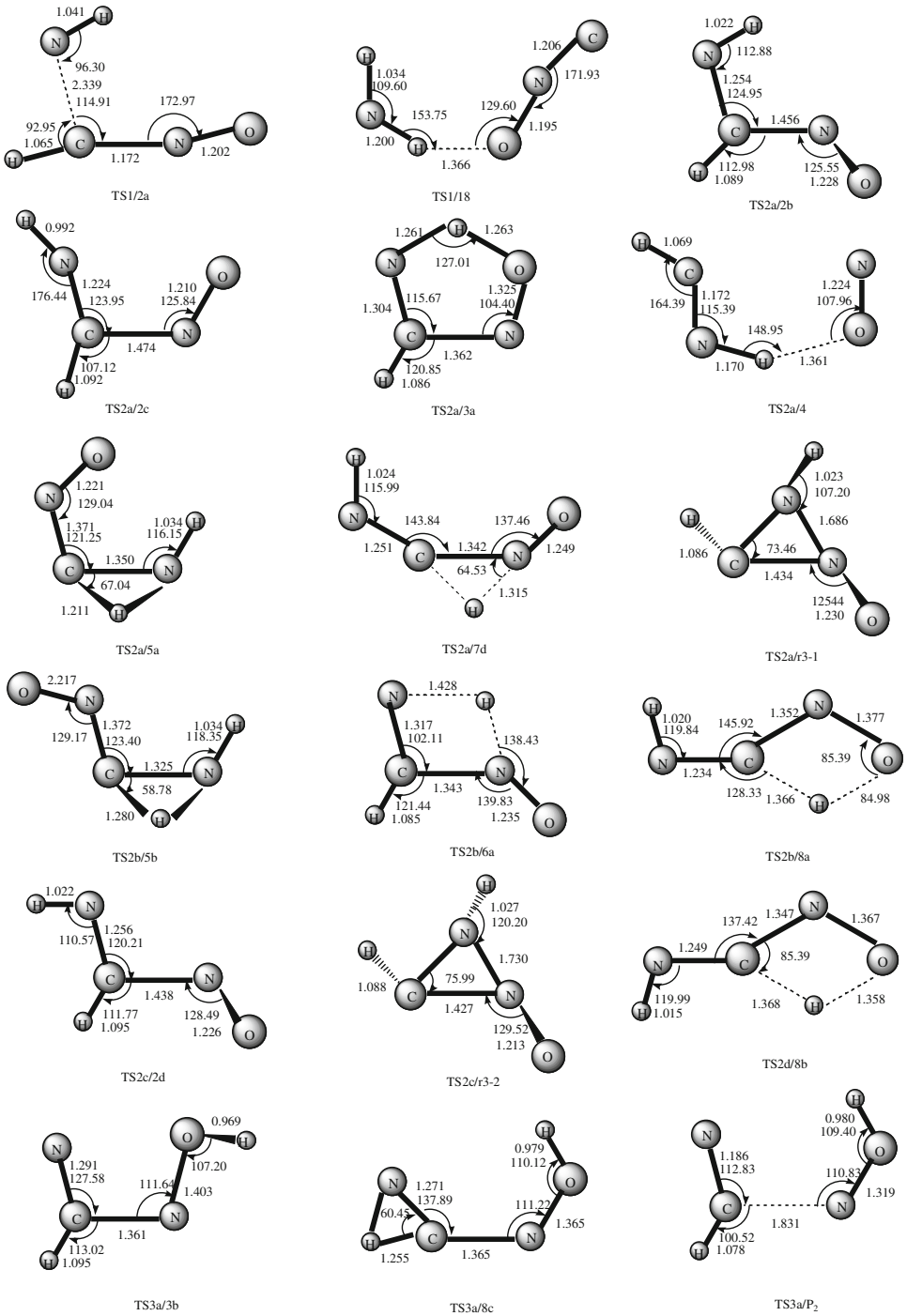

Fig. 3 The optimized structures of the transition states at the B3LYP/6-311++G(d,p) level. Distances are given in angstroms and angles in degrees

complex NOH···CNH **10** before the final product $\mathbf{P_3}$ as in **Path $\mathbf{P_3}$(1)**. On the other hand, **2d** undergoes 1,3-H-shift giving rise to HNCNOH **8b**, which can convert to **8c**, **8d**, and **8e**. Both **8b** and **8d** can dissociate to $\mathbf{P_3}$.

By comparison, we find that **Path $\mathbf{P_3}$(2)** is simpler than **Path $\mathbf{P_3}$(3)** and **Path $\mathbf{P_3}$(4)**. Then, **Path $\mathbf{P_3}$(2)** is expected to be competitive than the latter two pathways. Now, let us compare the feasibility of **Path $\mathbf{P_3}$(1)** and **Path $\mathbf{P_3}$(2)**. In **Path $\mathbf{P_3}$(1),** from **2a** to $\mathbf{P_3}$, three barriers need to be climbed, i.e., 8.4, 61.1, and 14.0 kcal/mol for **2a** → **2b**, **2b** → **8a**, and **8a** → **10** conversions, respectively. In **Path $\mathbf{P_3}$(2)**, four barriers need to be overcome, which are 22.0 (**2a** → **2c**), 8.3(**2c** → **2d**), 54.8 **2d** → **8b**), and 17.6 (**8b** → $\mathbf{P_3}$) kcal/mol. Moreover, **TS2b/8a** in **Path $\mathbf{P_3}$(1)** is 3.1 kcal/mol above the reactant. Then, we

Fig. 3 continued

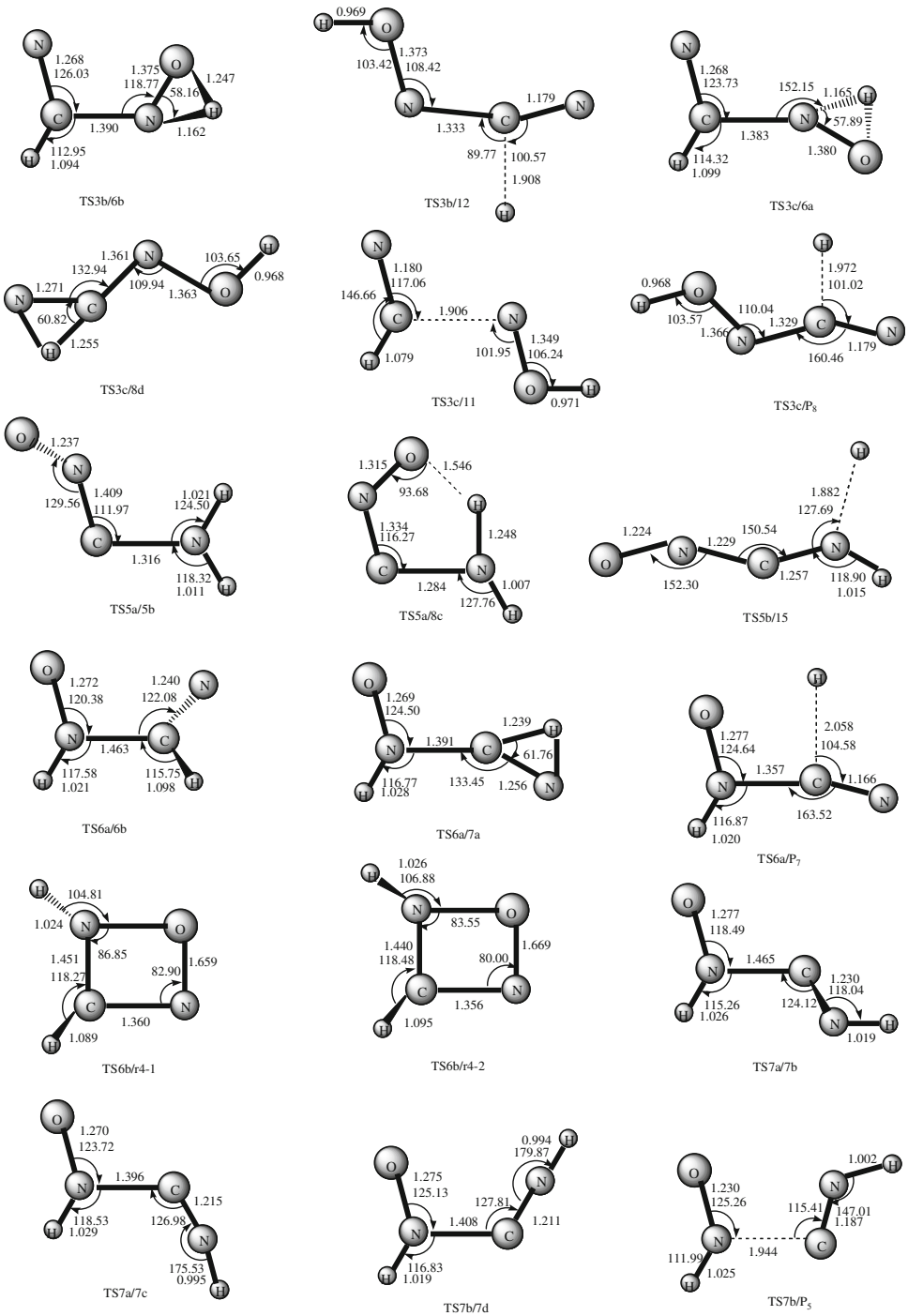

expect that **Path P_3(2)** may be the optimal channel to form $\mathbf{P_3}$.

3.2.3 Formation pathway of $P_5(^1HNC + {}^3HNO)$

As can be seen in Fig. 4a, four feasible pathways are associated with the formation of $\mathbf{P_5}$, which can be written as follows:

Path P_5(1) $\mathbf{R \rightarrow 1 \rightarrow 2a \rightarrow 2b \rightarrow 6a \rightarrow 7a \rightarrow 7b \rightarrow P_5}$
Path P_5(2) $\mathbf{R \rightarrow 1 \rightarrow 2a \rightarrow 2b \rightarrow 6a \rightarrow 7a \rightarrow 7b \rightarrow 7d \rightarrow P_5}$
Path P_5(3) $\mathbf{R \rightarrow 1 \rightarrow 2a \rightarrow 2b \rightarrow 6a \rightarrow 7a \rightarrow 7c \rightarrow 7d \rightarrow P_5}$
Path P_5(4) $\mathbf{R \rightarrow 1 \rightarrow 2a \rightarrow 2b \rightarrow 6a \rightarrow 7a \rightarrow 7c \rightarrow 7d \rightarrow 7b \rightarrow P_5}$

2b can undergo continuously 1,3- and 1,2-H-shift to form NCHNHO **6a**, then to HNCNHO **7a**. Subsequently, **7a** can convert to **7b**, **7c,** and **7d**. Both **7b** and **7d** can dissociate to $\mathbf{P_5}$.

Fig. 3 continued

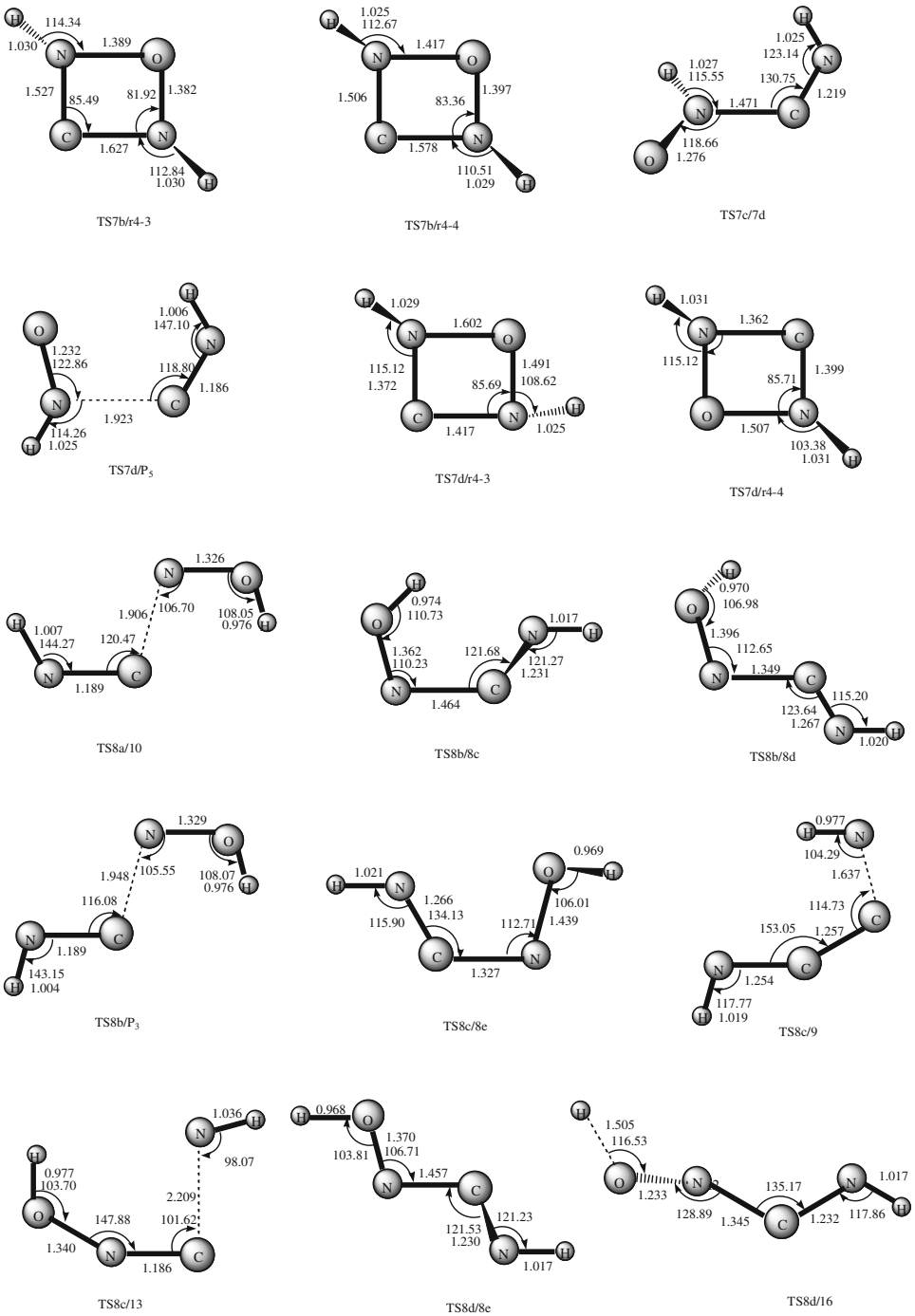

Obviously, **Path P_5 (1)** is simpler than the latter three paths; thus it is the optimal channel to form P_5. The conversion barriers for the steps **2b** → **6a**, **6a** → **7a**, **7a** → **7b** and **7b** → P_5 are 54.3, 45.8, 10.6 and 19.1 kcal/mol, respectively.

3.2.4 Formation pathways of $P_6(^2OH + {}^2HNCN)$

For product P_6, there are two pathways are energetically possible:

Path $P_6(1)$R → 2a → 2c → 2d → 8b → 8c → 9 → P_6

Path $P_6(2)$R → 2a → 2c → 2d → 8b → 8c → 8e → 9 → P_6

The formation of HNCNOH **8** (**8b**, **8c**, and **8e**) is the same as that in **Path P_3(2)**. Subsequently, **8c** can undergo either N–O rupture to form the weakly bound complex OH···NCNH **9** as in **Path P_6(1)** or successive N–O bond rotation and N–O bond fission to produce **8e**, then **9** as in **Path P_6(2)**. Finally, the weakly bound complex **9** can dissociate to P_6.

Fig. 3 continued

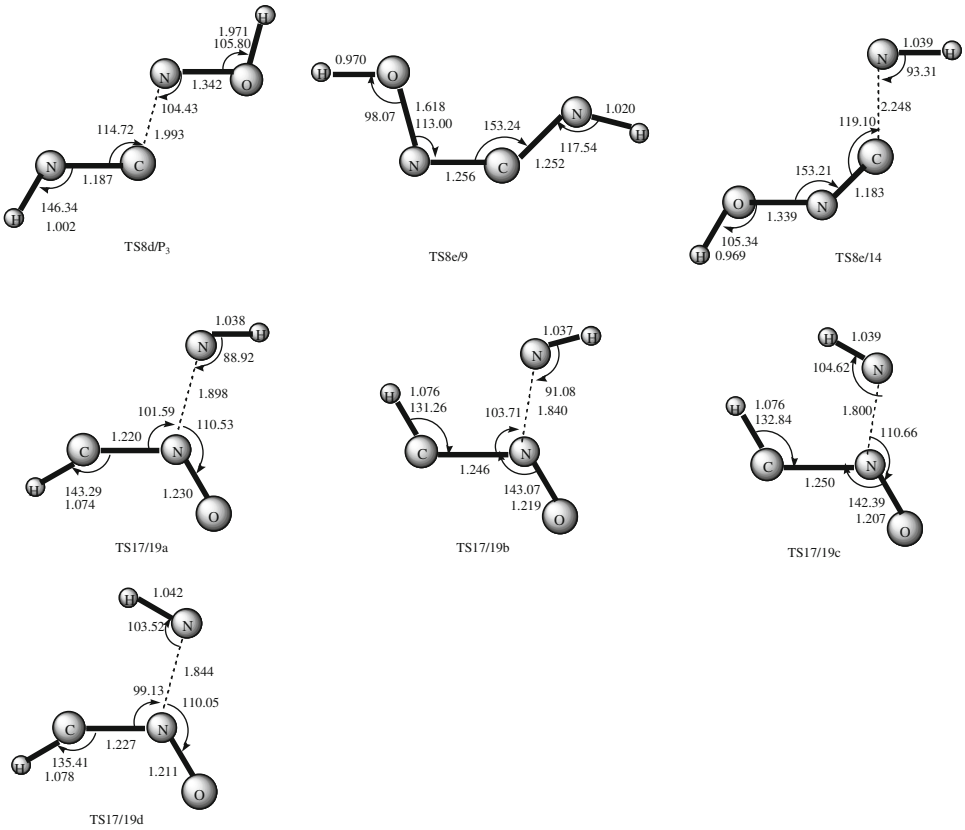

Surely, **Path P_6(1)** is simpler than **Path P_6(2)**: thus it should be the optimal channel to form $\mathbf{P_6}$.

3.2.5 *Unfavorable channels*

Now, let us consider the other isomerization and dissociation pathways of **2a**, **2b**, and **3a**. As shown in Fig. 4b, isomer HNCHNO **2a** can undergo either 1,2-H-shift to form $ONCNH_2$ **5a** or 2,3-H-shift lead to HNCNHO **7d**. However, these conversion transition states **TS2a/5a**, and **TS2a/7d** lie 18.6, and 19.0 kcal/mol above reactant **R**. Isomer HNCHNO **2b** can undergo 1,2-H-shift give rise to $ONCNH_2$ **5b** via **TS2b/5b** (11.2). Alternatively, **2b** takes successive 1,3-H and 1,2-H-shift interconversion to NC(H)NHO **6a**, and then to NC(H)NOH **3c**. But the conversion transition states **TS3c/6a** lies 6.7 kcal/mol higher in energy than reactant **R**. Isomer NCHNOH **3a** can undergo 1,2-H-shift to form HNCNOH **8c** via **TS3a/8c** with the relative energy of 7.1 kcal/mol. Obviously, all these processes are kinetically unfavorable. Though isomers **3c**, **5(5a,5b)**, **7d,** and **8d** can undergo further changes to form $\mathbf{P_2}(^1HCN + {}^3HON)$, $\mathbf{P_3}(^1HNC + {}^3HON)$, $\mathbf{P_4}(^2HNCNO + {}^2H)$, $\mathbf{P_5}(^1HNC + {}^3HNO)$, $\mathbf{P_6}(^2OH + {}^2HNCN)$, $\mathbf{P_8}(^2HONCN + {}^2H)$, and $\mathbf{P_9}(^1HONC + {}^3NH)$, these processes are not feasible for the $HCNO + {}^3NH$ reaction.

Besides the previously discussed chainlike isomers, we also obtain six cyclic isomers for $HCNO + {}^3NH$ reaction, that is, three-membered ring isomers r3-1 and r3-2 and four-membered ring isomers r4-1, r4-2, r4-3, and r4-4. However, as can be seen from Table 1, all these cyclic isomers lie much higher than **R** ($HCNO + {}^3NH$). Formation of the cyclic species is energetically inaccessible; therefore, we do not consider the further evolution pathways of these ring species.

4 Reaction mechanism

In the preceding sections, we have discussed the most feasible formation pathways for products $\mathbf{P_2}(^1HCN + {}^3HON)$, $\mathbf{P_3}(^1HNC + {}^3HON)$, $\mathbf{P_5}(^1HNC + {}^3HNO)$, and $\mathbf{P_6}(^2OH + {}^2HNCN)$. For easier understanding, they are listed again:

Path P_2(1)R → 1 → 2a → 3a → P_2

Path P_3(2)R → 1 → 2a → 2c → 2d → 8b → P_3

Path P_5(1)R → 1 → 2a → 2b → 6a → 7a → 7b → P_5

Path P_6(1)R → 1 → 2a → 2c → 2d → 8b → 8c → 9 → P_6

For these four reaction paths, the most competitive one should be **Path P_2(1)** because the energy barriers 39.2

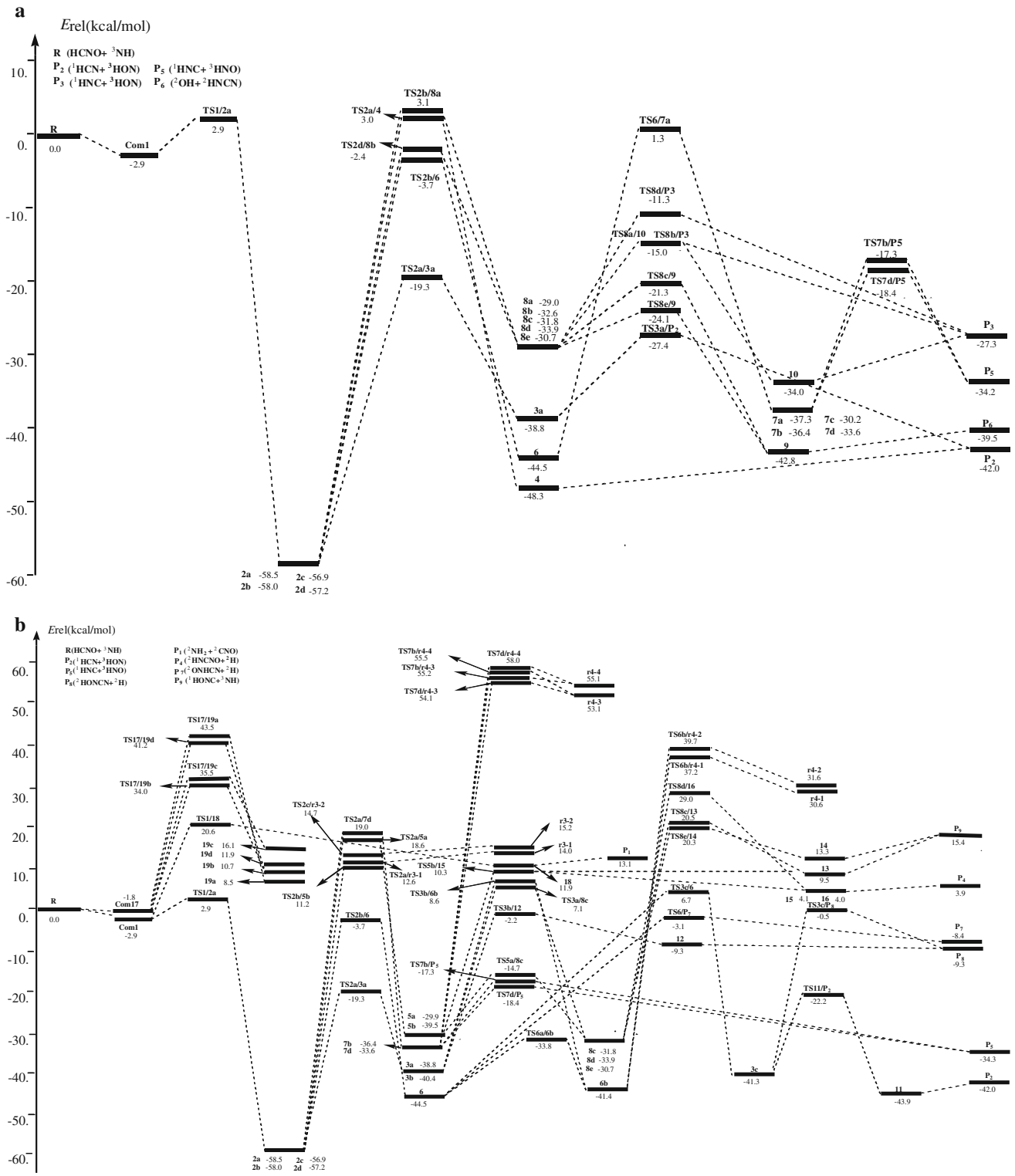

Fig. 4 **a** The potential energy surface (PES) of the favorable reaction channels for the HCNO + ^{3}NH reaction. *E*rel are the relative energies (kcal/mol). **b** The potential energy surface (PES) of the unfavorable reaction channels for the HCNO + ^{3}NH reaction. *E*rel are the relative energies (kcal/mol)

(**2a** → **3a**), and 11.4 (**3a** → **P$_2$**) kcal/mol in **Path P$_2$(1)** are much lower than 54.8 (**2d** → **8b**) kcal/mol in **Path P$_3$(2)**, 54.3 (**2b** → **6a**) and 45.8 (**6a** → **7a**) kcal/mol in **Path P$_5$(1)**, and 54.8 (**2d** → **8b**) kcal/mol in **Path P$_6$(1)**. With respect to the remaining three paths, formation of **P$_5$** via **Path P$_5$(1)** is the least feasible path since two high barriers

Table 1 Total (a.u.) and relative energies in parentheses (kcal/mol) of the reactants, products, and intermediates for the HCNO + ^{3}NH reaction

Species	B3LYP	G3B3	Species	B3LYP	G3B3
Reactant	–223.8693289	–223.6837326 (0.0)	7d	–223.9416279	–223.7372119 (–33.6)
P_1(^{2}NH$_2$ + ^{2}CNO)	–223.8535979	–223.6628088 (13.1)	8a	–223.9298503	–223.7299690 (–29.0)
P_2(^{1}HCN + ^{3}HON)	–223.9377265	–223.7507087 (–42.0)	8b	–223.9364865	–223.7357599 (–32.6)
P_3(^{1}HNC + ^{3}HON)	–223.9147754	–223.7272380 (–27.3)	8c	–223.9337969	–223.7344664 (–31.8)
P_4(^{2}HNCNO + ^{2}H)	–223.8664211	–223.6775826 (3.9)	8d	–223.9396802	–223.7377759 (-33.9)
P_5(^{1}HNC + ^{3}HNO)	–223.9308429	–223.7384614 (–34.3)	8e	–223.9338997	–223.7326254 (-30.7)
P_6(^{2}OH + ^{2}HNCN)	–223.9377829	–223.7466361 (–39.5)	9	–223.9449371	–223.7520179 (-42.8)
P_7(^{2}ONHCN + ^{2}H)	–223.8819060	–223.6971212 (–8.4)	10	–223.9272248	–223.7379107 (–34.0)
P_8(^{2}HONCN + ^{2}H)	–223.8809791	–223.6985435 (–9.3)	11	–223.9412751	–223.7537484 (–43.9)
P_9(^{1}HONC + ^{3}NH)	–223.8396160	–223.6592396 (15.4)	12	–223.8809514	–223.6986122 (–9.3)
1	–223.8746260	–223.6883697 (–2.9)	13	–223.8509218	–223.6685429 (9.5)
2a	–223.9806265	–223.7770271 (–58.5)	14	–223.8351860	–223.6625091 (13.3)
2b	–223.9795520	–223.7762408 (–58.0)	15	–223.8665036	–223.6772631 (4.1)
2c	–223.9782592	–223.7743972 (–56.9)	16	–223.8664165	–223.6774011 (4.0)
2d	–223.9784613	–223.7749266 (–57.2)	17	–223.8731821	–223.6866648 (–1.8)
3a	–223.9424821	–223.7455370 (–38.8)	18	–223.8558239	–223.6647773 (11.9)
3b	–223.9470944	–223.7480727 (–40.4)	19a	–223.8684249	–223.6701122 (8.5)
3c	–223.9484235	–223.7495000 (–41.3)	19b	–223.8637769	–223.6666128 (10.7)
4	–223.9495813	–223.7607540 (–48.3)	19c	–223.8538728	–223.6580733 (16.1)
5a	–223.9377986	–223.7314026 (–29.9)	19d	–223.8618347	–223.6647812 (11.9)
5b	–223.9549427	–223.7466064 (–39.5)	r3-1	–223.8619666	–223.6614298 (14.0)
6a	–223.9579021	–223.7547254 (–44.5)	r3-2	–223.8603512	–223.6595038 (15.2)
6b	–223.9530584	–223.7497857 (–41.4)	r4-1	–223.8280126	–223.6350202 (30.6)
7a	–223.9489360	–223.7432422 (–37.3)	r4-2	–223.8266826	–223.6333423 (31.6)
7b	–223.9476691	–223.7417510 (–36.4)	r4-3	–223.7918503	–223.5993280 (53.1)
7c	–223.9359528	–223.7319259 (–30.2)	r4-4	–223.7885048	–223.5959964 (55.1)

Table 2 Total (a.u.) and relative energies in parentheses (kcal/mol) of the transition states for the HCNO + ^{3}NH reaction

Species	B3LYP	G3B3	Species	B3LYP	G3B3
TS1/2a	–223.8695230	–223.6790427 (2.9)	TS6a/P_7	–223.8774967	–223.6886123 (–3.1)
TS1/18	–223.8481516	–223.6508705 (20.6)	TS6b/r4-1	–223.8160536	–223.6244652 (37.2)
TS2a/2b	–223.9650732	–223.7636051 (–50.1)	TS6b/r4-2	–223.8119957	–223.6204249 (39.7)
TS2a/2c	–223.9461937	–223.7418683 (–36.5)	TS7a/7b	–223.9272351	–223.7262947 (–26.7)
TS2a/3a	–223.9099455	–223.7145654 (–19.3)	TS7a/7c	–223.9269618	–223.7230897 (–24.7)
TS2a/4	–223.9191157	–223.6789618 (3.0)	TS7b/7d	–223.9293061	–223.7251872 (–26.0)
TS2a/5a	–223.8541279	–223.6540536 (18.6)	TS7b/P_5	–223.9131469	–223.7112606 (–17.3)
TS2a/7d	–223.8544971	–223.6534001 (19.0)	TS7b-r4-3	–223.7880074	–223.5957222 (55.2)
TS2a/r3-1	–223.8614167	–223.6635869 (12.6)	TS7b-r4-4	–223.7873222	–223.5953455 (55.5)
TS2b/5b	–223.8679170	–223.6659042 (11.2)	TS7d/P_5	–223.9150797	–223.7131334 (-18.4)
TS2b/6a	–223.8881557	–223.6895528 (–3.7)	TS7d-r4-3	–223.7904153	–223.5975593 (54.1)
TS2b/8a	–223.8772565	–223.6788620 (3.1)	TS7d-r4-4	–223.7831942	–223.5913592 (58.0)
TS2c/2d	–223.9621296	–223.7612512 (–48.6)	TS8a/10	–223.9033466	–223.7075733 (–15.0)
TS2c/r3-2	–223.8590743	–223.6603747 (14.7)	TS8b/8c	–223.9097330	–223.7130184 (–18.4)
TS2d/8b	–223.8868701	–223.6875442 (–2.4)	TS8b/8d	–223.9165056	–223.7180497 (–21.5)
TS3a/3b	–223.9260649	–223.7309324 (–29.6)	TS8b/P_3	–223.9015426	–223.7076257 (–15.0)
TS3a/8c	–223.8627427	–223.6724078 (7.1)	TS8c/8e	–223.9111657	–223.7135929 (–18.7)
TS3a/P_2	–223.9216541	–223.7274729 (–27.4)	TS8c/9	–223.9196282	–223.7176668 (–21.3)
TS3b/12	–223.8739198	–223.6872344 (–2.2)	TS8c/13	–223.8381032	–223.6510439 (20.5)

Table 2 continued

Species	B3LYP	G3B3	Species	B3LYP	G3B3
TS3b/6b	–223.8644753	–223.6699973 (8.6)	TS8d/8e	–223.9157338	–223.7175543 (–21.2)
TS3c/6a	–223.8675920	–223.6731259 (6.7)	TS8d/16	–223.8414193	–223.6374991 (29.0)
TS3c/8d	–223.8718019	–223.6785092 (3.3)	TS8d/P_3	–223.8971609	–223.7016949 (–11.3)
TS3c/11	–223.9134393	–223.7191282 (–22.2)	TS8e/9	–223.9255997	–223.7221463 (–24.1)
TS3c/P_8	–223.8767630	–223.6845569 (–0.5)	TS8e/14	–223.8386559	–223.6513082 (20.3)
TS5a/5b	–223.9238393	–223.7184074 (–21.8)	TS17/19a	–223.8121920	–223.6143335 (43.5)
TS5a/8c	–223.9050142	–223.7072049 (–14.7)	TS17/19b	–223.8266299	–223.6294989 (34.0)
TS5b/15	–223.8642813	–223.6672788 (10.3)	TS17/19c	–223.8240225	–223.6272277 (35.5)
TS6a/6b	–223.9385114	–223.7376403 (–33.8)	TS17/19d	–223.8166489	–223.6181053 (41.2)
TS6a/7a	–223.8783110	–223.6815858 (1.3)			

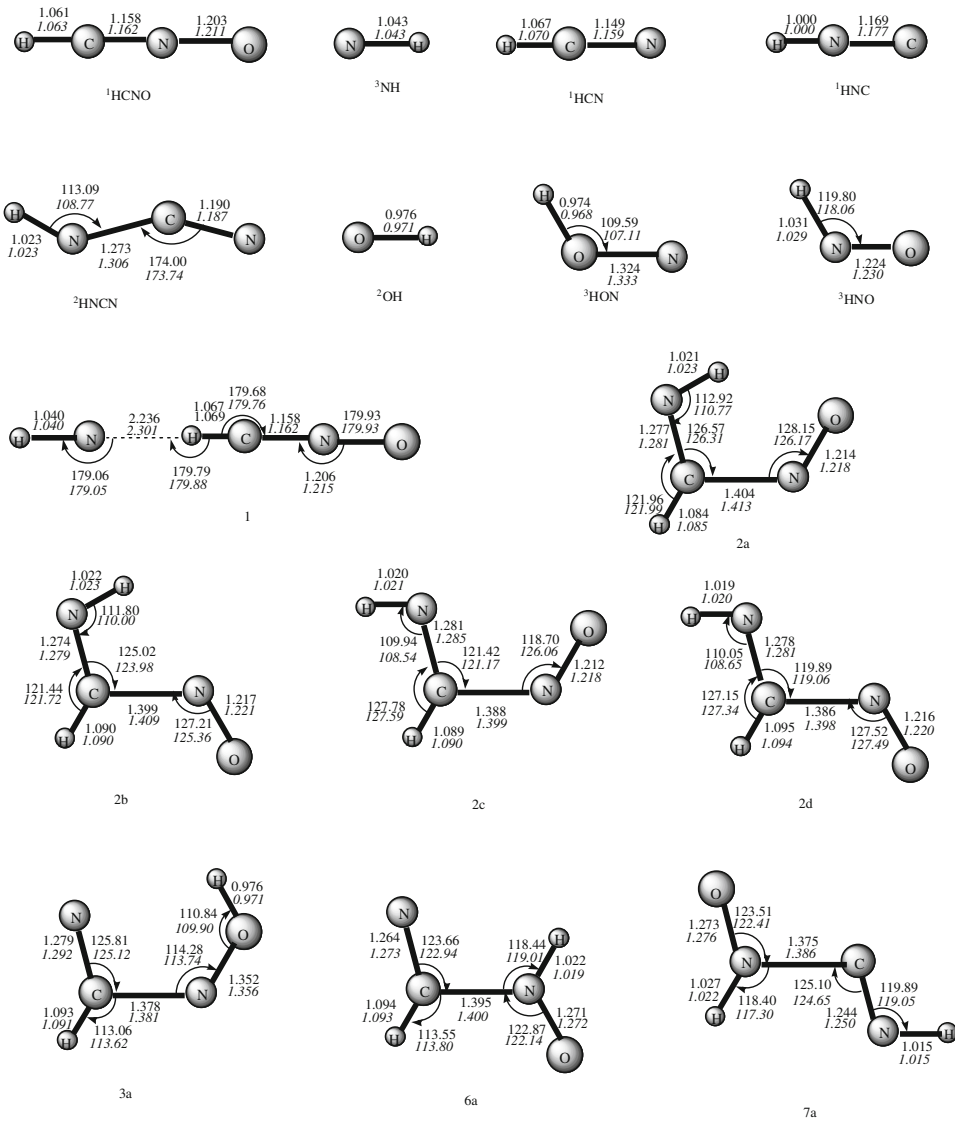

Fig. 5 The optimized structures of the species involved in the most feasible channel at B3LYP/6-311++G(d,p) and QCISD/6-311++G(d,p)(in italic) levels

Fig. 5 continued

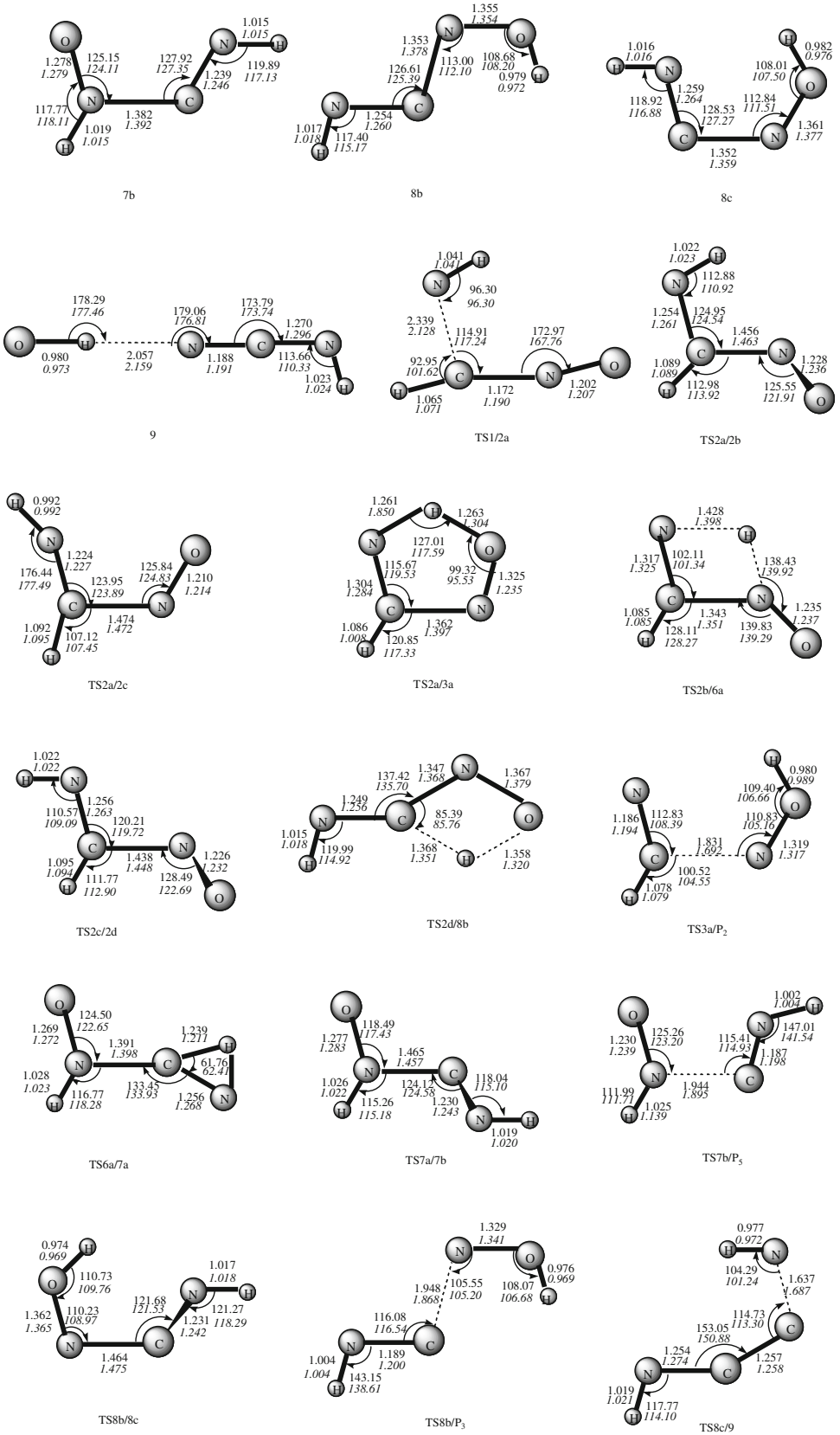

Table 3 Total (a.u.) and relative energies in parentheses (kcal/mol) of the critical structures for the HCNO + ^{3}NH reaction

Species	G3B3//B3LYP	G3B3//QCISD
Reactant	–223.6837326 (0.0)	–223.6844775 (0.0)
P_2(^{1}HCN + ^{3}HON)	–223.7507087 (–42.0)	–223.7508133 (–41.0)
P_3(^{1}HNC + ^{3}HON)	–223.7272380 (–27.3)	–223.7270083 (–26.7)
P_5(^{1}HNC + ^{3}HNO)	–223.7384614 (–34.3)	–223.7384261 (–33.9)
P_6(^{2}OH + ^{2}HNCN)	–223.7466361 (–39.5)	–223.7466881 (–39.2)
1	–223.6883697 (–2.9)	–223.6890464 (–2.9)
2a	–223.7770271 (–58.5)	–223.7766053 (–57.8)
2b	–223.7762408 (–58.0)	–223.7757009 (–57.2)
2c	–223.7743972 (–56.9)	–223.7739661 (–56.2)
2d	–223.7749266 (–57.2)	–223.7744673 (–56.5)
3a	–223.745537 (–38.8)	–223.7451642 (–38.1)
6a	–223.7547254 (–44.5)	–223.7543278 (–43.8)
7a	–223.7432422 (–37.3)	–223.7429398 (–36.7)
7b	–223.741751 (–36.4)	–223.7415926 (–35.8)
8b	–223.7357599 (–32.6)	–223.7355235 (–32.0)
8c	–223.7344664 (–31.8)	–223.7342907 (–31.3)
9	–223.7520179 (–42.8)	–223.7522064 (–42.5)
TS1/2a	–223.6790427 (2.9)	–223.6759778 (5.3)
TS2a/2b	–223.7636051 (–50.1)	–223.7639262 (–49.9)
TS2a/2c	–223.7418683 (–36.5)	–223.7413035 (–35.7)
TS2a/3a	–223.7145654 (–19.3)	–223.7136450 (–18.3)
TS2b/6a	–223.6895528 (–3.7)	–223.6894005 (–3.1)
TS2c/2d	–223.7612512 (–48.6)	–223.7614083 (–48.3)
TS2d/8b	–223.6875442 (–2.4)	–223.6875231 (–1.9)
TS3a/P_2	–223.7274729 (–27.4)	–223.7270107 (–26.7)
TS6a/7a	–223.6815858 (1.3)	–223.6806924 (2.4)
TS7a/7b	–223.7262947 (–26.7)	–223.7246098 (–25.2)
TS7b/P_5	–223.7112606 (–17.3)	–223.7103908 (–16.3)
TS8b/8c	–223.7130184 (–18.4)	–223.7126487 (–17.7)
TS8c/9	–223.7176668 (–21.3)	–223.7177860 (–20.9)

need to be climbed in **Path P_5(1)**, while in **Path P_3(2)** and **Path P_6(1)**, only one high barrier need to be climbed. In addition, we notice that **Path P_3(2)** is simpler than **Path P_6(1)**: thus, **Path P_3(2)** may be slightly competitive than **Path P_6(1)**.

As a result, as reflected in the final product distributions, we predict that a total of four kinds of products may be observed. **P_2**(^{1}HCN + ^{3}HON) is the most favorable product, **P_3**(^{1}HNC + ^{3}HON) and **P_6**(^{2}OH + ^{2}HNCN) are lesser followed products, but much less competitive than **P_2**. **P_5**(^{1}HNC + ^{3}HNO) may be the least feasible product.

5 Reliability assessment

We performed additional calculations for the critical species of some reaction channels using the higher level and cost-expensive QCISD/6-311++G(d,p) method. It should be pointed out that HN···HCNO **Com1** is in fact a first-order saddle point at QCISD/6-311++G(d,p) level because it has an imaginary frequency (17i). We tried to find a true isomer with all real frequencies, but did not succeed because in all cases we obtained the two separated fragments (HCNO + ^{3}NH). Thus, the relative energy of **Com1** is just a crude estimation of the corresponding true isomer.

As shown in Fig. 5, the structure parameters at the two levels are generally in good agreement with each other. Most important, the relative energies of these 30 species calculated at G3B3//B3LYP/6-311++G(d,p) and G3B3//QCISD/6-311++G(d,p) levels are close to each other with the largest deviation 2.4 kcal/mol of **TS1/2a**. Thus we expect that the G3B3//B3LYP/6-311++G(d,p) method can provide reliable mechanistic information for the HCNO + ^{3}NH reaction.

6 Conclusion

A detailed quantum chemical study is performed on the mechanism of the HCNO + ^{3}NH reaction. The main calculation results can be summarized as follows: In various possible entrance channels, the carbon to nitrogen attack to form HNCHNO **2a** is most favorable, while the other attacks are considerably barrier-consumed. Starting from **2a**, four kinds of products **P_2**(^{1}HCN + ^{3}HON), **P_3**(^{1}HNC + ^{3}HON), **P_5**(^{1}HNC + ^{3}HNO), and **P_6**(^{2}OH + ^{2}HNCN) can be obtained. Among these four products, **P_2** is the most favorable product. **P_3** and **P_6** are the second and third feasible products, whereas **P_5** is the least feasible product. The present paper is the first study of HCNO + ^{3}NH reaction, and our calculations may present a useful base for future product determination both experimentally and theoretically.

Acknowledgments This work is supported by the National Natural Science Foundation of China (Nos. 20773048).

References

1. Miller JA, Klippenstein SJ, Glarborg P (2003) Combust Flame 135:357. doi:10.1016/j.combustflame.2003.07.002
2. Zhang WC, Du BN, Feng CJ (2004) J Mol Struct Theochem 679:121. doi:10.1016/j.theochem.2004.04.012
3. Eshchenko G, Kocher T, Kerst C, Temps F (2007) Chem Phys Lett 356:181. doi:10.1016/S0009-2614(02)00387-1
4. Bauerle S, Klatt M, Wagner HG, Bunsen-Ges B (1995) Phys Chem 99:97
5. Grussdorf J, Temps F, Wagner HG, Bunsen-Ges B (1997) Phys Chem 101:34
6. Meyer JP, Hershberger JF (2005) J Phys Chem B 109:8363. doi:10.1021/jp040503h

7. Vereecken L, Sumathy R, Carl SA, Peeters J (2001) Chem Phys Lett 344:400. doi:10.1016/S0009-2614(01)00818-1
8. Tokmakov IV, Moskaleva LV, Paschenko DV, Lin MC (2003) J Phys Chem A 107:1066. doi:10.1021/jp022024t
9. Rim KT, Hershberger JF (2000) J Phys Chem A 104:293. doi:10.1021/jp9922209
10. Eickhoff U, Temps F (1999) Phys Chem Chem Phys 1:243. doi:10.1039/a807258b
11. Nguyen MT, Boullart W, Peeters J (1994) J Phys Chem 98:8030. doi:10.1021/j100084a019
12. Schulze G, Koja O, Winnewisser BP, Winnewisser M (2000) J Mol Struct 517:307. doi:10.1016/S0022-2860(99)00260-4
13. Albert S, Albert KK, Winnewisser M, Winnewisser BP (2001) J Mol Struct 599:347. doi:10.1016/S0022-2860(01)00823-7
14. Feng WH, Hershberger JF (2008) Chem Phys Lett 457:307. doi:10.1016/j.cplett.2008.04.012
15. Feng WH, Hershberger JF (2007) J Phys Chem A 111:10654. doi:10.1021/jp075636s
16. Miller JA, Durant P, Glarborg P (1998) Proc Combust Inst 27:235
17. Wang S, Yu JK, Ding DJ, Sun CC (2007) Theor Chem Acc 118:337. doi:10.1007/s00214-007-0262-1
18. Feng WH, Meyer JP, Hershberger JF (2006) J Phys Chem A 110:4458. doi:10.1021/jp058305t
19. Li BT, Zhang J, Wu HS, Sun GD (2007) J Phys Chem A 111:7211. doi:10.1021/jp072637b
20. Feng WH, Hershberger JF (2007) J Phys Chem A 111:3831. doi:10.1021/jp066036g
21. Zhang WC, Du BN, Feng CJ (2007) Chem Phys Lett 442:1. doi:10.1016/j.cplett.2007.05.041
22. Feng WH, Hershberger JF (2006) J Phys Chem A 110:12184. doi:10.1021/jp0650073
23. Pang JL, Xie HB, Zhang SW, Ding YH, Tang AQ (2008) J Phys Chem A 112:5251. doi:10.1021/jp709700u
24. Wang S, Yu JK, Ding DJ, Sun CC (2008) Chem J Chin Univ Chin 29:365
25. Haynes BS (1977) Combust Flame 28:81. doi:10.1016/0010-2180(77)90010-4
26. Haynes BS (1977) Combust Flame 28:113. doi:10.1016/0010-2180(77)90017-7
27. Lyon R (1987) En iron. Sci Technol 21:231. doi:10.1021/es00157a002
28. Radford HE, Litvak MM (1975) Chem Phys Lett 34:561. doi:10.1016/0009-2614(75)85562-X
29. Wayne FD, Radford HE (1976) Mol Phys 32:1407. doi:10.1080/00268977600102771
30. Bernath PF, Amano T (1982) J Mol Spectrosc 95:359. doi:10.1016/0022-2852(82)90135-7
31. Brazier CR, Ram RS, Bernath PF (1986) J Mol Spectrosc 120:381. doi:10.1016/0022-2852(86)90012-3
32. Adam L, Hack W, Zhu H, Qu ZW, Schinke R (2005) J Chem Phys 122:114301. doi:10.1063/1.1862615
33. Takahashi K, Takayanagi K (2007) J Mol Struct Theochem 817:153. doi:10.1016/j.theochem.2007.04.032
34. Takahashi K, Takayanagi T (2006) Chem Phys Lett 429:399. doi:10.1016/j.cplett.2006.08.109
35. Xu ZF, Sun JZ (1998) J Phys Chem A 102:1194. doi:10.1021/jp972959n
36. Xu ZF, Li SM, Yu YX, Li ZS, Sun CC (1999) J Phys Chem A 103:4910. doi:10.1021/jp984499j
37. Du B, Zhang W, Mu L, Feng C (2007) J Mol Struct Theochem 816:21. doi:10.1016/j.theochem.2007.03.034
38. Redondo P, Pauzat F, Ellinger Y (2006) Planet Space Sci 54:181. doi:10.1016/j.pss.2005.10.008
39. Mackie J, Bacskay GB (2005) J Phys Chem A 109:11967. doi:10.1021/jp0544585
40. Frisch MJ, Trucks GW, Schlegel HB, Scusera GE, Robb MA, Cheeseman JR, Zakrzewski VG, Montgomery JA Jr, Stratmann RE, Burant JC, Dapprich S, Millam JM, Daniels AD, Kudin KN, Strain MC, Farkas O, Tomasi J, Barone V, Cossi M, Cammi R, Mennucci B, Pomelli C, Adamo C, Clifford S, Ochterski J, Petersson GA, Ayala PY, Cui Q, Morokuma K, Malick DK, Rabuck AD, Raghavachari K, Foresman JB, Cioslowski J, Ortiz JV, Stefanov BB, Liu G, Liashenko A, Piskorz P, Komaromi I, Gomperts R, Martin RL, Fox DJ, Keith T, Al-Laham MA, Peng CY, Nanayakkara A, Gonzalez C, Challacombe M, Gill PMW, Johnson B, Chen W, Wong MW, Andres JL, Gonzalez C, Head-Gordon M, Replogle ES, Pople JA (1998) Gaussian 98, Revision A.6. Gaussian, Inc., Pittsburgh
41. Frisch MJ, Trucks GW, Schlegel HB, Scuseria GE, Robb MA, Cheeseman JR, Montgomery JA Jr, Vreven T, Kudin KN, Burant JC, Millam JM, Iyengar SS, Tomasi J, Barone V, Mennucci B, Cossi M, Scalmani G, Rega N, Petersson GA, Nakatsuji H, Hada M, Ehara M, Toyota K, Fukuda R, Hasegawa J, Ishida M, Nakajima T, Honda Y, Kitao O, Nakai H, Klene M, Li X, Knox JE, Hratchian HP, Cross JB, Bakken V, Adamo C, Jaramillo J, Gomperts R, Stratmann RE, Yazyev O, Austin AJ, Cammi R, Pomelli C, Ochterski JW, Ayala PY, Morokuma K, Voth GA, Salvador P, Dannenberg JJ, Zakrzewski VG, Dapprich S, Daniels AD, Strain MC, Farkas O, Malick DK, Rabuck AD, Raghavachari K, Foresman JB, Ortiz JV, Cui Q, Baboul AG, Clifford S, Cioslowski J, Stefanov BB, Liu G, Liashenko A, Piskorz P, Komaromi I, Martin RL, Fox DJ, Keith T, Al-Laham MA, Peng CY, Nanayakkara A, Challacombe M, Gill PMW, Johnson B, Chen W, Wong MW, Gonzalez C, Pople JA (2004) Gaussian 03, Revision B.03. Gaussian, Inc., Wallingford
42. Curtiss LA, Raghavachari K, Redfern PC, Rassolov V, Pople JAJ (1998) Chem Phys 109:7764
43. Boboul AG, Curtiss LA, Redfern PC, Raghavachari KJ (1999) Chem Phys 110:7650